Islamic Azad University
Mashhad Branch

# Petrogenetic Evolution of Plio-Quaternary Mafic Lavas in Nehbandan (East Iran)

**Mohammad Reza Ghasempour[1*], Javad Mehdipour Ghazi[2], Habib Biabangard[3], Rahim Dabiri[4]**

*1. Faculty of Natural Resources and Earth Science, Shahrekord University, Shahrekord, Iran*
*2. Faculty of Earth Science, Shahid Beheshti University, Tehran, Iran*
*3. Department of Geology,Sistan and Baluchestan University, Zahedan, Iran*
*4. Department of Geology, Mashhad Branch, Islamic Azad University, Mashhad, Iran*
Received 22 September 2014; accepted 20 August 2014

**Abstract**

Both the Sistan Suture Zone of eastern Iran and the Nehbandan Fault contain Plio-Quaternary Nehbandan mafic lavas. Positive anomalies in the large ion lithophile elements (LILE) and negative anomalies in Nb exist in these mafic lavas. This indicates the occurrence of subduction magmatism and post-collision volcanism. Petrologic and geochemical analyses distinguished two groups of lava. Group I contains alkaline basalts with a slight depletion in Nb while Group II contains sub-alkaline basaltic andesite to andesite with a sharp depletion in Nb. Geochemical studies show that fractional crystallization and crustal contamination played an important part in the evolution of the Nehbandan lavas. Group II, however, was more greatly affected than Group I. Geochemical studies also indicate that these lavas may have been generated due to a low degree of partial melting (<5%) of garnet and the spinel-bearing lithospheric mantle; Group I shows more garnet than spinel while Group II shows the opposite. The research carried out for this paper suggests that the Plio-Quaternary Nehbandan mafic lavas were formed as a result of slab detachment or delamination and domination, an extensional condition correlated to the thinning of the crust and lithosphere in the Sistan Collision Zone. These conditions are concomitant with localized stretching along the Nehbandan Fault and the upwelling of magma forming mafic lavas.

***Keywords:*** *Plio-Quaternary lavas, geochemical, post-collision volcanism, Lithospheric source, Sistan Suture Zone.*

## 1. Introduction

This paper describes the Plio-Quaternary magmatism of the Nehbandan area, presents a petrologic and geochemical study of the Nehbandan lavas and discusses the geochemical evidence for the magmatic evolution of these lavas. The Nehbandan area is part of the Sistan Suture Zone of eastern Iran and was mapped using a 1:250,000 scale [1]. Plio-Quaternary lavas cover parts of the Sistan Zone and give useful insight into the processes that controlled the geodynamic and magmatic evolution of this zone. The Nehbandan area is covered extensively with ophiolitic Mesozoic to Early Eocene and Cenozoic metamorphosed clastic sedimentary rocks (Fig.1). These ophiolitic rocks were previously studied by Saccani et al. [2]. They believed that the ophiolitic rocks were related to the supra-subduction zone and hypothesized that the closing of the Sistan Ocean was due to an inter-oceanic subduction. Arjmandzadeh and Hazrati suggested that the magmatic rocks in the Sistan Zone are Eocene and Oligocene and that the eastern portion of the Lut Block shows calc-alkaline and adakite trends [3,4]. A careful study of these rocks, which erupted during the Pliocene and Quaternary periods, showed them to be andesite to basalt in composition following a N-S trend (Fig.1).

*Corresponding author.
*E-mail address (es): ghasempour_1984@yahoo.com*

## 2. Geological Setting

There are various ophiolitic complexes along the Sistan Suture Zone which form a discontinuous N–S trending belt from Zahedan to Birjand indicating that the zone is the remains of an oceanic crust. Most recent studies are of the belief that the subduction of the oceanic lithosphere played a major role in the tectonic evolution of this area [3]. There are currently three geodynamic models that consider subduction. One refers to structural evidence and proposes that subduction occurred beneath the Afghan Block [2,5]. Another considers high calc-alkaline magmatism and proposes that the oceanic lithosphere was dragged under the Lut Block [6,7]. Recently, Arjmandzadeh et al. suggested a two-sided subduction in this zone that could explain the tectonic, magmatic and metallogenic characteristics of the Lut Block [3].

The Sistan Suture Zone contains a Cretaceous-Tertiary orogenic belt, part of the complex Alpine-Himalayan collision zone [5, 8]. Stocklin suggested that this orogenic belt is separated from the Afghan Block in the east (Fig. 1) [9]. Due to an increasing convergence rate between the Neo-Tethys and the Central Iranian Microcontinent (CIM), the Sistan Sea (between CIM and Afghan Block) began to close during the Campanian to Paleocene (83-55 Ma). According to studies done by Tirrul et al. [5], the Sistan Suture Zone is composed of two parts: the older Ratuk Complex to

the east and the younger Neh Complex to the west. The Ratuk Complex is an anticlinorium of Upper Cretaceous flysch-like sediments and Cretaceous ophiolites. The eastern portion of the Ratuk Complex contains exposed rocks in the basement of the Afghan Block that consist of Lower Cretaceous limestone uncomfortably overlying Proterozoic rocks. The Neh Complex is Coniacian to Early Eocene in age (89-49 Ma). Tirrul et al. [5] suggested that the Sistan Suture Zone switched to a more westerly position. The Sefidabeh forearc basin uncomfortably overlies these two complexes. This basin consists of unmetamorphosed clastic sediments of Campanian to Early Eocene age (71-49 Ma) [5]. The Sistan Suture Zone is also characterized by the widespread occurrence of calc-alkaline and alkaline volcanic rocks ranging from Upper Cretaceous to Neogene in age. Upper Cretaceous–Paleocene calc-alkaline volcanic rocks form outcrops in the eastern margin of the Sefidabeh basin [10]. Additionally, syntectonic to post-tectonic intrusions formed after the closure of the Sistan Suture Zone in the Late Eocene–Early Miocene [10, 11]. Lithological relationships show that ophiolite emplacement occurred during the Late Cretaceous but deep-water sedimentation continued until the Early Eocene. Following this, the collision between the Lut and Afghan Blocks resulted in the closure of the basin and the regional uplift of the terrenes of the Sistan Suture Zone.

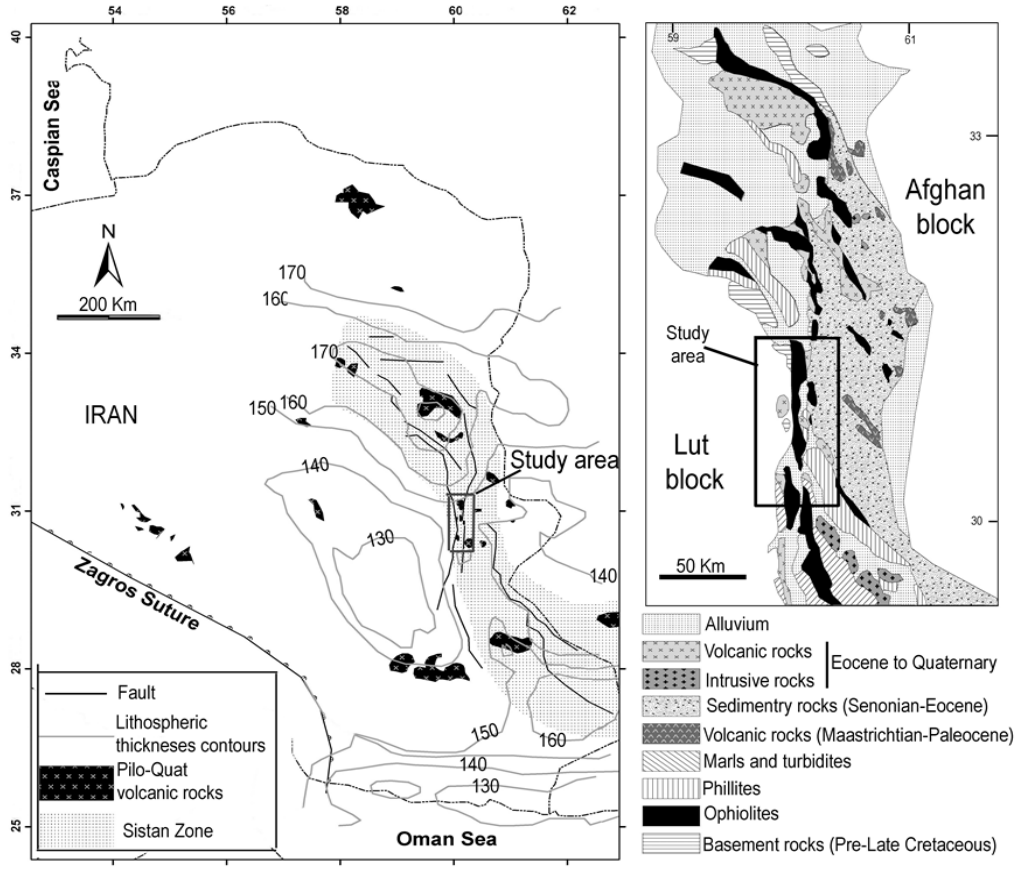


Fig. 1: (a) Late Cenozoic volcanic centers [12], active faults [13] and lithospheric thickness contours in Eastern Iran [14] (b) Geological sketch map of the northern portion of the Sistan Suture Zone (modified after [5] )

## 3. Petrography

The volcanic rocks in this study are basalt, basaltic andesite and andesite in composition. Basaltic rocks are dominant and show a porphyritic texture with phenocrysts of plagioclase, olivine and clinopyroxene. Plagioclase minerals are found in abundance in the phenocrysts and are characterized by multiple twinning. They contain small inclusions of glass and groundmass material zonally arranged or clustered in the central part of the crystal. Occasionally they show signs of corrosion and are surrounded by glass (Fig. 2a). The Clinopyroxene minerals are euhedral and often show oscillatory zoning (Fig. 2b). The abundance of olivine, found in several of the thin rocks, varies from 1% to 10%, forms a fine-grained groundmass and more rarely, phenocrysts. The olivine phenocrysts are occasionally skeletal, most likely due to rapid quenching, corrosion and breakage (Fig. 2c). Some samples show a glomeroporphyric texture composed of

an accumulation of olivine and clinopyroxene. The plagioclase in the andesitic rocks exhibits a high occurrence of sieve textures in addition to well-defined zoning marked by concentric zones commonly rich in glass and/or opaque inclusions. These rocks contain large amphibole crystals that occur as the main ferromagnesian phenocrysts (up to 2 mm in size) and often alter to opaque iron oxides (Fig. 2d). The groundmass texture of the lavas varies from holocrystalline to aphanitic and shows an interstitial to fluidal texture. This variation may be related to differential degrees of cooling and crystallization at various levels of the ascending magmas. The groundmass is composed of plagioclase and hornblende as the main minerals, with biotite, pyroxenes and iron oxides as accessory minerals. The primary structures consisting of ropy lava, vesicles and amygdales filled with calcite, chlorite and columnar joints, show a high level of preservation.

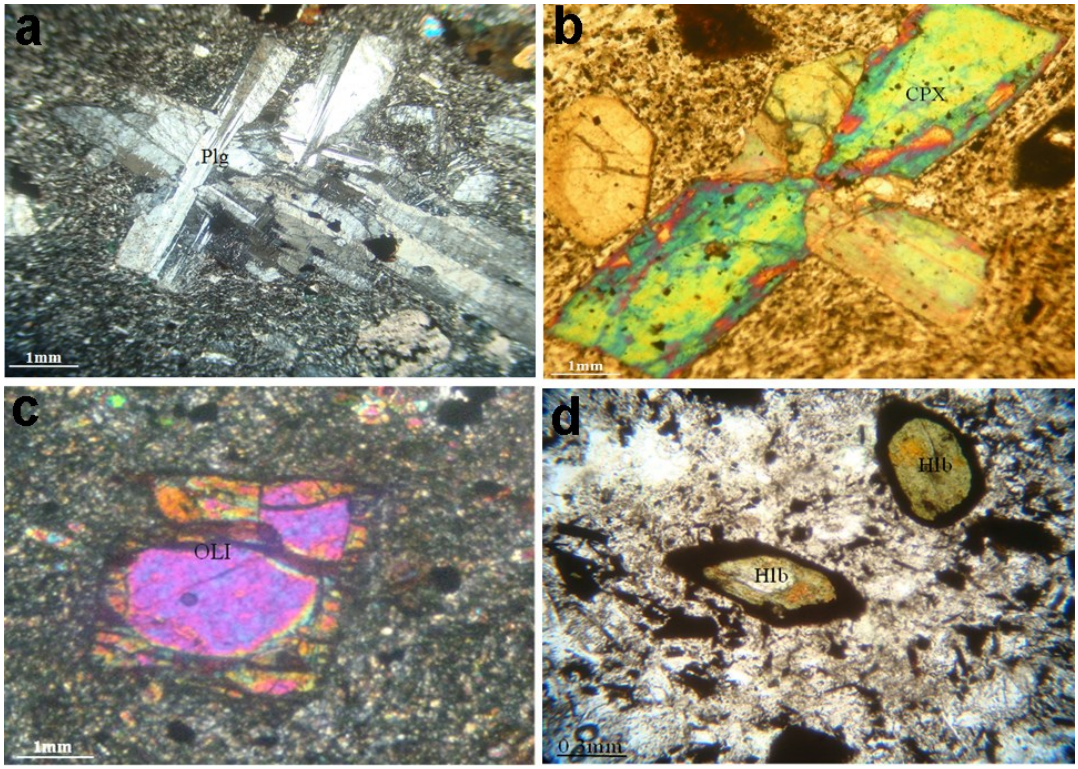


Fig. 2: Microphotography of volcanic rocks in the study area (a) Clustered plagioclases in alkaline basalt (b) large phenocrysts of clinopyroxene in alkaline basalt (c) corroded and broken olivine phenocrysts in alkaline basalt (d) opaque and altered amphiboles to opaque iron oxides in subalkaline andesite

## 4. Geochemistry

### 4.1. Analytical Techniques

Approximately 80 samples were collected from different mafic rocks. In order to correctly characterize their chemical compositions, 12 of the least altered samples were chosen for major, trace and Rare Earth Elements (REE) analysis. Samples used for whole rock analysis were crushed and powdered using agate ball-mills. Major, trace and REE were determined through Inductively Coupled Plasma Mass Spectrometry (ICP-MS) and Inductively Coupled Plasma - Optical Emission Spectrometry (ICP-OES) at the ALS CEMEX Company of Canada using fused glass and pressed powder discs. Representative chemical analysis for major, trace and rare earth elements are presented in Table 1.

### 4.2. Whole Rock Chemistry

Based on microscopic studies two types of lava, basalt and basaltic andesite to andesite were identified. Geochemical analysis identified two lava subgroups. Group I, containing alkaline basaltic rocks (8 samples) and Group II containing subalkaline basaltic andesite to andesite (4 samples). In the Nb/Y- $Zr/TiO_2$ Diagram (Fig. 3), 4 samples of the Nehbandan lava plot in the subalkaline mafic rock field (andesite, basalt and basaltic andesite) and 8 samples in the alkaline basalt field. The average potassium oxide ($K_2O$) and magnesium oxide (MgO) content of Group II is higher than Group I while the amount of titanium dioxide ($TiO_2$) and phosphorus pentoxide ($P_2O_5$) is higher in Group I (Table 1)

.

Table 1: Results of whole-rock analyses of the Pilo-Quaternary Nehbandan mafic lavas

| | Group I | | | | | | | | Group II | | | |
|---|---|---|---|---|---|---|---|---|---|---|---|---|
| | Wt% | | | | | | | | | | | |
| $SiO_2$ | 50.9 | 53.3 | 49.1 | 54.9 | 55.5 | 57 | 55.3 | 53.7 | 47.8 | 52.6 | 47.9 | 50 |
| $Al_2O_3$ | 15.1 | 15.85 | 15.05 | 15.85 | 15.9 | 15.8 | 16.1 | 14.45 | 10.85 | 13.6 | 13 | 13.8 |
| $Fe_2O_3$ | 8.08 | 6.6 | 7.86 | 6.21 | 6.3 | 5.72 | 6.79 | 7.72 | 9.16 | 7.97 | 7.92 | 8.59 |
| CaO | 9.3 | 9.12 | 9.54 | 7.06 | 7.47 | 6.51 | 7.17 | 8.11 | 8.19 | 8.76 | 9.86 | 8.83 |
| MgO | 4.56 | 3.42 | 4.89 | 3.45 | 3.59 | 3 | 3.07 | 5.25 | 15.7 | 6.71 | 7.55 | 13.1 |
| $Na_2O$ | 4.76 | 5.33 | 4.74 | 5.37 | 5.66 | 5.85 | 5.32 | 4.28 | 2.04 | 2.62 | 3.75 | 2.96 |
| $K_2O$ | 1.36 | 1.24 | 1.64 | 1.46 | 1.54 | 1.54 | 1.6 | 1.4 | 2.03 | 2.49 | 2.07 | 1.22 |
| $TiO_2$ | 1.84 | 1.62 | 1.82 | 1.64 | 1.71 | 1.54 | 1.68 | 1.78 | 0.62 | 0.67 | 1.02 | 0.75 |
| MnO | 0.12 | 0.09 | 0.11 | 0.1 | 0.1 | 0.09 | 0.1 | 0.13 | 0.15 | 0.13 | 0.13 | 0.14 |
| $P_2O_5$ | 1.08 | 1.02 | 1.2 | 0.89 | 0.93 | 1.05 | 0.91 | 0.87 | 0.28 | 0.32 | 0.7 | 0.24 |
| $Cr_2O_3$ | 0.02 | 0.01 | 0.01 | 0.01 | 0.01 | 0.01 | 0.01 | 0.02 | 0.19 | 0.05 | 0.04 | 0.14 |
| SrO | 0.17 | 0.19 | 0.22 | 0.15 | 0.16 | 0.17 | 0.16 | 0.18 | 0.07 | 0.07 | 0.16 | 0.06 |
| BaO | 0.05 | 0.08 | 0.07 | 0.05 | 0.05 | 0.05 | 0.05 | 0.05 | 0.07 | 0.08 | 0.15 | 0.05 |
| LOI | 0.8 | 2.29 | 2.8 | 1.19 | 1.8 | 0.3 | 2 | 1.59 | 1.32 | 2.1 | 3.88 | 0.3 |
| Total | 98.1 | 100 | 99.1 | 98.3 | 100.5 | 98.6 | 100.5 | 99.5 | 98.5 | 98.2 | 98.1 | 100 |
| | ppm | | | | | | | | | | | |
| Ba | 471 | 707 | 623 | 389 | 418 | 433 | 395 | 397 | 647 | 745 | 1345 | 427 |
| Ce | 122.5 | 117.5 | 144 | 97.4 | 96.8 | 95.3 | 96 | 98.3 | 41.9 | 43.4 | 156 | 42.2 |
| Co | 25.4 | 19.8 | 25.7 | 20.7 | 20.5 | 18.5 | 22.3 | 31.2 | 54.4 | 27.5 | 31.3 | 58.5 |
| Cr | 110 | 90 | 90 | 60 | 50 | 70 | 50 | 170 | 1370 | 340 | 270 | 960 |
| Cs | 0.78 | 0.92 | 1.01 | 0.56 | 0.9 | 0.55 | 2.04 | 4.17 | 1.26 | 0.41 | 2.62 | 0.92 |
| Cu | 886 | 108 | 69 | 50 | 39 | 89 | 49 | 136 | 84 | 95 | 109 | 66 |
| Dy | 4.43 | 3.7 | 4.19 | 3.56 | 3.42 | 3.29 | 3.45 | 4.31 | 2.98 | 3.3 | 5.74 | 3.08 |
| Er | 2.06 | 1.6 | 1.91 | 1.67 | 1.63 | 1.54 | 1.62 | 2.26 | 1.79 | 2.02 | 2.58 | 1.75 |
| Eu | 2.43 | 2.16 | 2.58 | 2.09 | 2.08 | 2.03 | 2.06 | 2.18 | 1.15 | 1.14 | 3.34 | 1.25 |
| Ga | 20.3 | 20.5 | 21 | 21 | 21 | 20.8 | 20.8 | 19.8 | 12.4 | 14.7 | 19 | 16 |
| Gd | 7.68 | 6.97 | 8.39 | 6.1 | 5.92 | 6 | 5.96 | 6.43 | 3.91 | 4.22 | 10.8 | 3.87 |
| Hf | 5.2 | 5.2 | 5.3 | 5.1 | 4.9 | 5.4 | 5 | 5.1 | 2 | 2.2 | 5.7 | 2.3 |
| Ho | 0.74 | 0.59 | 0.71 | 0.61 | 0.59 | 0.57 | 0.6 | 0.77 | 0.57 | 0.61 | 0.87 | 0.58 |
| La | 58.1 | 58 | 69 | 47.2 | 47.4 | 46.2 | 47.9 | 46.2 | 21.2 | 22 | 80 | 21.2 |
| Lu | 0.17 | 0.13 | 0.16 | 0.16 | 0.15 | 0.14 | 0.16 | 0.25 | 0.21 | 0.19 | 0.18 | 0.21 |
| Mo | 2 | 2 | 2 | 2 | 2 | 2 | 2 | 2 | 2 | 2 | 2 | 2 |
| Nb | 31.1 | 27.4 | 32.1 | 29.1 | 29.4 | 25.9 | 29.3 | 29.7 | 5.7 | 4.9 | 16.5 | 6.4 |
| Nd | 54.7 | 50.9 | 63 | 42 | 41.5 | 41.5 | 41.7 | 44.6 | 20.2 | 21.4 | 70.6 | 20.2 |
| Ni | 46 | 42 | 43 | 34 | 36 | 42 | 38 | 96 | 495 | 56 | 58 | 366 |
| Pb | 8 | 7 | 12 | 22 | 12 | 8 | 16 | 12 | 9 | 11 | 17 | 8 |
| Pr | 13.95 | 13 | 16.15 | 11.15 | 11.15 | 11 | 11.1 | 11.6 | 4.72 | 5.07 | 17.65 | 4.8 |
| Rb | 24.9 | 19.7 | 27.4 | 20.7 | 21.4 | 20.7 | 22.2 | 39.8 | 60 | 57.4 | 35 | 29 |
| Sm | 9.32 | 8.65 | 10.25 | 7.12 | 7.13 | 6.92 | 7.1 | 7.92 | 4.43 | 4.56 | 14.1 | 4.29 |
| Sn | 2 | 2 | 2 | 1 | 1 | 1 | 2 | 2 | 1 | 1 | 2 | 1 |
| Sr | 1310 | 1440 | 1750 | 1115 | 1125 | 1255 | 1175 | 1365 | 596 | 586 | 1380 | 486 |
| Ta | 1.8 | 1.6 | 1.8 | 1.4 | 1.4 | 1.2 | 1.4 | 1.6 | 0.4 | 0.6 | 1.1 | 0.4 |
| Tb | 0.92 | 0.8 | 0.94 | 0.84 | 0.82 | 0.8 | 0.8 | 0.94 | 0.52 | 0.53 | 1.17 | 0.54 |
| Th | 4.82 | 5.02 | 5.9 | 5.66 | 5.27 | 4.39 | 5.19 | 5.28 | 5.99 | 6.59 | 18.9 | 4.85 |
| Tl | 0.5 | 0.5 | 0.5 | 0.5 | 0.5 | 0.5 | 0.5 | 0.5 | 0.5 | 0.5 | 0.5 | 0.5 |
| Tm | 0.23 | 0.17 | 0.2 | 0.19 | 0.18 | 0.17 | 0.17 | 0.26 | 0.23 | 0.16 | 0.18 | 0.22 |
| U | 0.76 | 1.18 | 1.11 | 1.16 | 1.36 | 0.77 | 1.69 | 1.95 | 1.1 | 1.47 | 3.31 | 0.97 |
| V | 196 | 136 | 189 | 139 | 158 | 102 | 152 | 232 | 190 | 213 | 262 | 204 |
| W | 1 | 1 | 1 | 1 | 2 | 1 | 2 | 2 | 1 | 4 | 4 | 1 |
| Y | 20.2 | 16.6 | 19.8 | 15.5 | 15.2 | 14.7 | 15.4 | 20.8 | 16.3 | 19 | 27.6 | 16.4 |
| Yb | 1.44 | 1.1 | 1.35 | 1.17 | 1.1 | 1.08 | 1.12 | 1.69 | 1.5 | 1.82 | 1.93 | 1.54 |
| Zn | 128 | 122 | 146 | 169 | 121 | 113 | 124 | 121 | 81 | 76 | 102 | 89 |
| Zr | 219 | 235 | 225 | 238 | 237 | 253 | 239 | 221 | 72 | 84 | 226 | 89 |

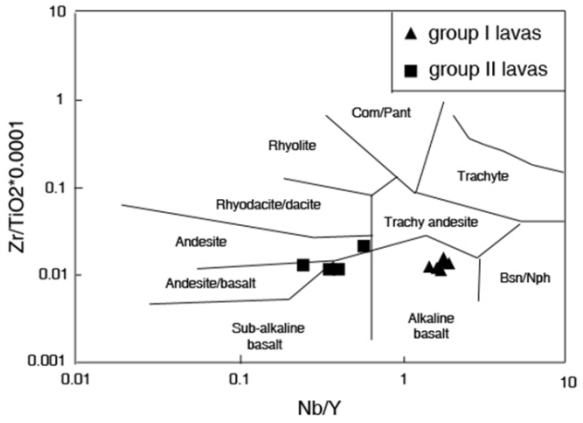


Fig. 3: Geochemical discrimination diagram from [15]

The MgO content for most of the lavas is lower than the primary melts of the mantle peridotite; only two samples from Group II show MgO>8%. Klein & Langmuir , Niu & Batiza and Langmuir et al. noted that high amounts of sodium oxide ($Na_2O$) in the basaltic glass could be an indication of a lower degree of mantle melting and vice versa [16,17 and 18]. Therefore, the oxide amounts found in the Nehbandan Group I lavas (4.2-5.8 wt %) compared to Group II (2-3.7 wt %), indicate that lavas from Group II are the result of a higher degree of mantle source melting relative to Group I.

The primitive mantle-normalized multi-element plot [19] for the two groups of lava are enriched with cesium (Cs), barium (Ba), uranium (U) and lead (Pb) but depleted in niobium (Nb) (Figs. 4 a,b). Group I is characterized by a slight depletion in Nb relative to Group II. The normalized trace element patterns for both groups show distinctive spikes. This may be associated with Ocean Island Basalts (OIB), particularly the peaks in Large Ion Lithophile (LIL) elements (Figs. 4c,d). Additionally, negative anomalies in Nb, titanium (Ti) and Heavy Rare Earth Elements (HREE) were observed. Chondrite normalized REE patterns in the two groups are characterized by a relatively flat pattern in HREE and relatively enriched Middle Rare Earth Element (MREE) to HREE pattern. This suggests that the samples from Group II are slightly more depleted in MREE and Light Rare Earth Elements (LREE) than Group I (Figs. 4e,f). Variable patterns are common in post-collision rocks. This may reflect the presence of a heterogeneous source for the generation of these rocks. The negative Nb and Ti anomalies show the role of subducted liquids in mantle metasomatism [21].

The tectonic setting of the Nehbandan lavas was investigated using the diagram proposed by Muller and Groves [22]. Most of the samples plotted in a post-collision magmatic arc (Fig. 5). Three samples from the two groups of lava are located in the continental-arc field (near the line separating post-collision magmatic arc and continental-arc field). Low amounts of phosphorus (P) along with high amounts of potassium (K) in the rocks from Group II, may be related to high potassic post collision rocks [22] and P mobilization in the lavas due to alteration. According to the Loss Of Ignition (LOI) wt % some samples are plotted in the continental arc field (Fig. 5).

## 5. Discussion

It is important to consider the possible effects of crustal contamination before trying to determine the source region characteristics and their melting histories. The continental crust exhibits relatively high Th/Ce (thorium/cerium) ratios (0.15) [23] whereas mantle-derived magmas have low Th/Ce ratios (0.02-0.5). Low Th/Ce ratios suggest that crustal contamination did not play a significant role in the generation of the magma [24]. Lavas contained in Group I exhibit low Th/Ce (0.039-0.058) ratios while Th/Ce ratios in Group II (0.11-0.15) are high. These ratios suggest that slab-derived components and crustal contamination played a role of in the generation of the magma in Group II.

Normalized trace element patterns show distinctive spikes. This is likely due to the presence of continental crust, especially the peaks in Ba and Th. Ba, Th, and Nb are used to identify the subduction component in lavas [25]. These elements are highly incompatible but behave in a similar manner during melting and fractional crystallization. Ba and Th are significantly partitioned into siliceous melts, while Ba is extensively partitioned into aqueous fluids derived from the subducted slab. Ratios in the studied samples show that the lavas are influenced by different subduction-related components. Group I shows lower Th/Ta ratios (2.6-4) compared to Group II (10.9-17.1) and slightly higher Ba/Th ratios (Group I: 68.7-140.8, Group II 71.1-113). These amounts indicate that fluids resulting from the dehydration of subducted materials played a major role in the generation of the Nehbandan lavas; Group I lavas show more an effect than lavas from Group II.

The geochemical data confirms that fractional crystallization played a role in the evolution of the Nehbandan lavas. The abundance of phenocrysts and the range of MgO (3 to 15.7%) in the Nehbandan lavas (Group I: 6.7 to 15.7% and Group II: 3 to 5.2%) may be the result of crystal fractionation during the ascent of the magma. The amount of MgO present in Group II shows that the lavas in this group experienced more variable amounts of fractional crystallization than Group I. Olivine and clinopyroxene are the dominant fractionating phase minerals. The diagram comparing calcium oxide/aluminum oxide ($CaO/Al_2O_3$) versus iron oxide/magnesium oxide (FeO/MgO) (Fig. 6) was used to evaluate the influence of mineral fractionation on the samples. The positive correlation of $CaO/Al_2O_3$ with FeO/MgO seen in Group I is consistent with clinopyroxene/amphibole fractionation. In contrast, the

spreading of the Group II lavas along a horizontal trend is most likely the result of olivine fractionation. Due to the amounts of $TiO_2$ and phosphorus pentoxide ($P_2O_5$) in the Group II lavas, apatite, FeO and TiO may also have played an important part in the fractionation phases.

The ratios of (Th/Yb) and (Ta/Yb) can be considered independent of fractional crystallization and/or partial melting and thus highlight source variations and crustal assimilation (e.g. [26]). Basaltic magma derived from the mantle asthenosphere, Depleted MORB (Mid Ocean Ridge Basalt) Mantle (DMM), plume asthenosphere or mantle lithosphere was enriched by small degree melts from the asthenosphere; all lie within or close to a diagonal mantle array defined by constant Th/Ta ratios. However, source region metasomatism caused by subduction resulted in an enrichment of Th with respect to Ta. Because the subduction components typically carry Th but not Ta or Yb, the Th/Yb ratios are higher than the Ta/Yb ratios. Crustal contamination may also increase the Th/Yb ratio relative to the Ta/Yb ratio because of the higher abundances of Th relative to Ta in crustal rocks.

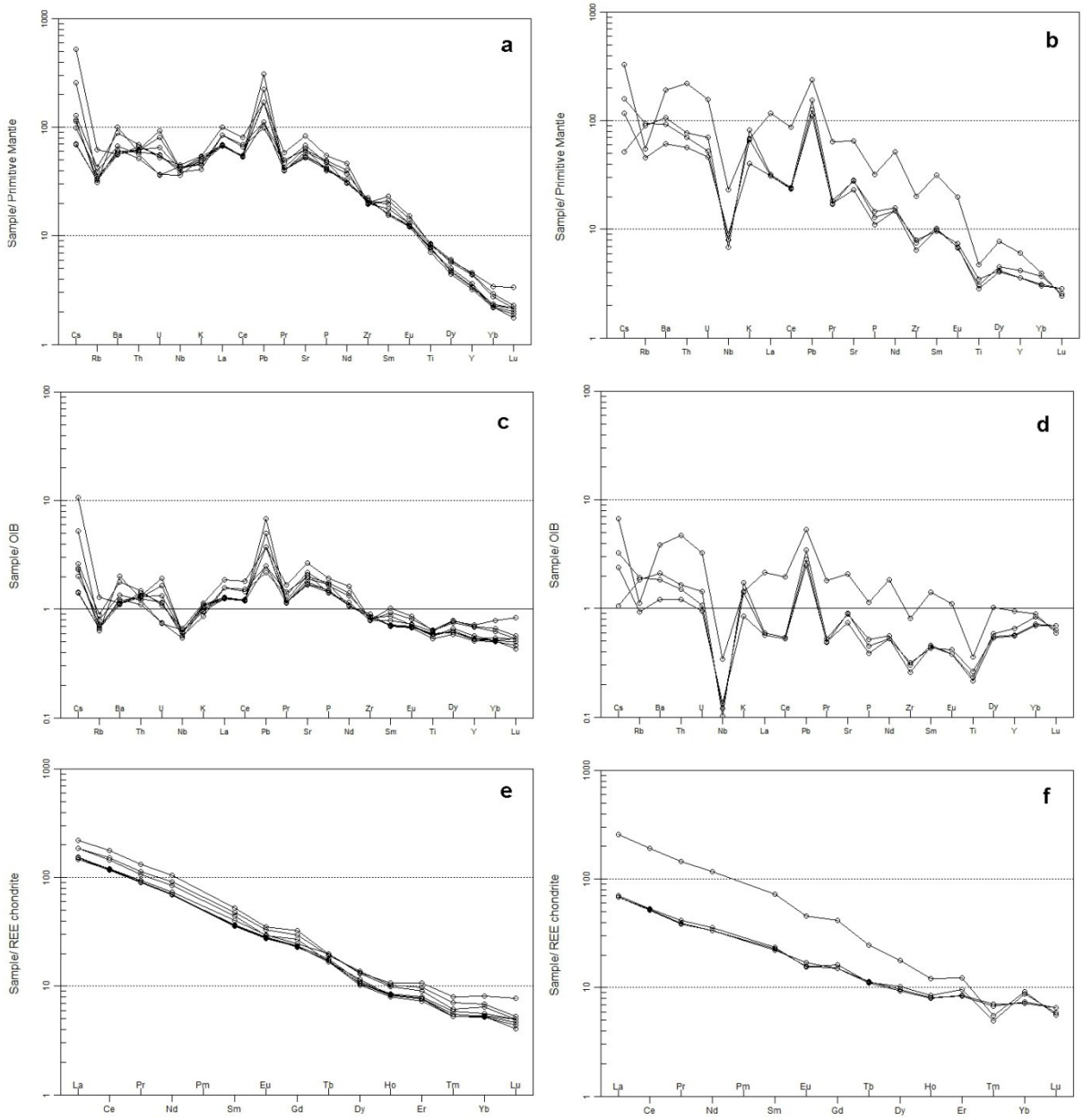


Fig. 4: Normalized patterns for primary mantle [19], OIB [19] and Chondrite [20] for Group I (a,c,e) and Group II (b,d,f).

Therefore, the plot comparing Th/Yb versus Ta/Yb (Fig. 7) provides useful constraints concerning the source characteristics involved in the creation of the Nehbandan lavas. Mantle enriched by small volume partial melts is displaced along the melt enrichment and within-plate trend in the direction of high Th/Yb and Ta/Yb ratios. Figure 7 shows that both groups are enriched by subduction zone components. These ratios show that there is a higher level of enrichment in the lavas of Group II. Figure 7 also shows that the magma from Group I was derived from an enriched mantle source and was produced by a smaller degree of partial melting compared to the magma from Group II. Samples taken from Group II in general and one sample in particular, show signs of Assimilation-Fractional Crystallization (AFC) (Fig.7).

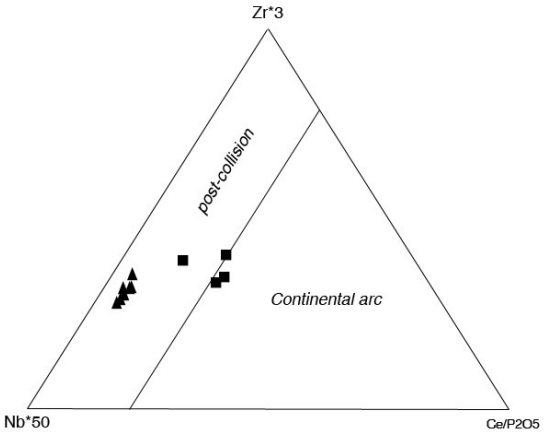


Fig. 5: $Ce/P_2O_5$–Nb*50–Zr*3 Diagram separating post collision rocks from active continental margin rocks from [22] (symbol key can be found in Fig. 3).

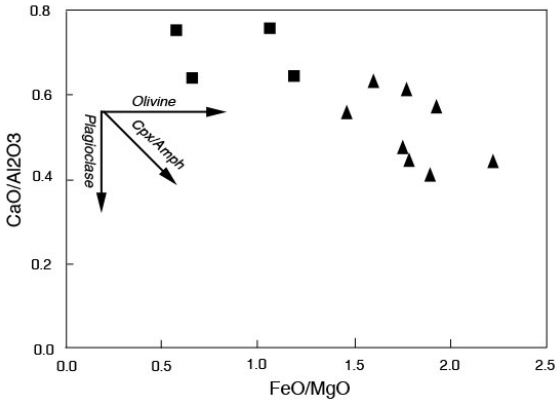


Fig. 6: $CaO/Al_2O_3$ versus $FeO_t/MgO$ Diagram for Nehbandan volcanic rocks

Neither lanthanum (La) nor samarium (Sm) are affected by variations in the source mineralogy (e.g. garnet or spinel) and thus are able to provide information concerning the bulk chemical composition of the source. Because Yb is compatible with garnet but not with clinopyroxene, the Sm/Yb ratio can be used to constrain the source mineralogy of the alkaline magmas [27]. A plot comparing Sm/Yb to La/Sm is able to distinguish between garnet and spinel peridotite melting sources [28]. Partial melting of a garnet peridotite source produces melts with a higher Sm/Yb ratio than a spinel peridotite source.

The residual mineralogy and degree of partial melting in the Sistan Suture Zone mantle can be further characterized using REE abundances and ratios found in the basaltic magma. Two different reference compositions were used to define whether DMM or primitive mantle was the most likely mantle array. DMM is believed to represent the convecting asthenospheric mantle with regard to the composition of the hypothetical depleted MORB source proposed by McKenzie and O'Nions [29]. Primitive mantle (Sun and McDonough [19]) is representative of the initial mantle composition prior to MORB formation and depletion. The Figure 8 diagram shows that most of the alkaline rocks in Group I have La/Sm ratios greater than those that can be generated by direct melting of DMM, even when the degree of partial melting is small (<5%). This diagram also shows that Group I and one sample from Group II are displaced from the spinel lherzolite trend. These samples show higher Sm/Yb ratios and plot between the melting trajectories drawn for garnet lherzolite and garnet-spinel lherzolite. The remaining samples from Group II were formed as a result of low melting trajectories drawn for spinel lherzolite and garnet-spinel lherzolite. The plot indicates the presence of garnet residue at various levels in the source region. The geochemical characteristics, such as the Nb/Y ratios, indicate that the Nehbandan lavas were generated from a lithospheric source. Nehbandan lavas show Nb/Y ratios of less than 2; this reveals that these lavas were not generated from an asthenospheric source. The geochemistry of the Nehbandan lavas is different from OIB suggesting that the Nehbandan lavas do not have an asthenospheric origin.

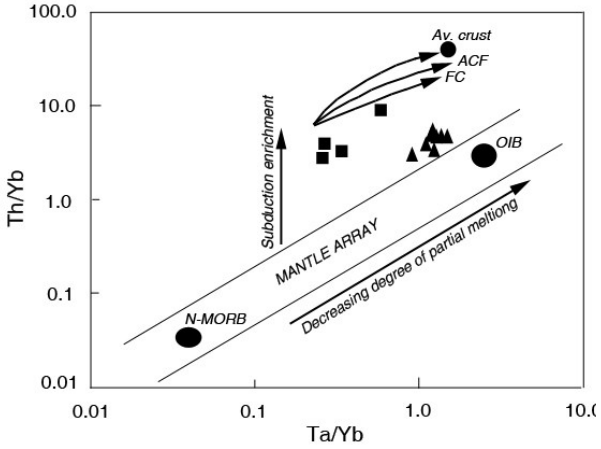


Fig. 7: Th/Yb versus Ta/Yb Diagram[30] for mafic lavas from Nehbandan area (symbol key can be found in Fig. 3)

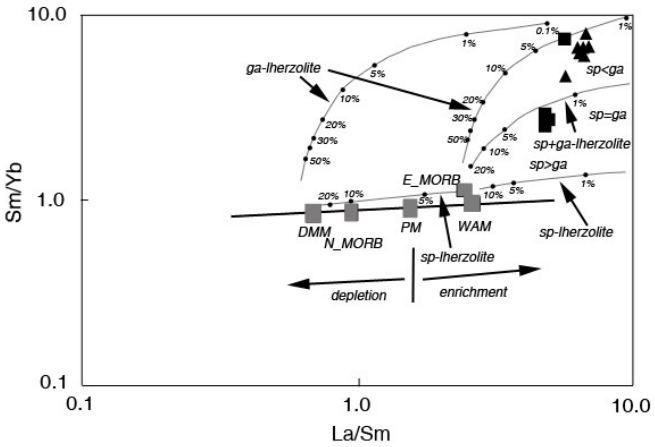


Fig. 8: Sm/Yb versus La/Sm plots showing REE concentrations for alkaline magma(s), considering source mineralogy and degree of partial melting [27]. Melt curves (or lines) were obtained using the non-modal batch melting equations of [31], (symbol key can be found in Fig. 3).

## 6. Conclusions

Petrographic and geochemical data from the Nehbandan lavas shows the existence of two types of lava: alkaline basaltic lavas (Group I) and calc-alkaline basaltic-andesite to andesite lavas (Group II). The geochemistry shows the effects of crustal contamination, fractional crystallization and subduction zone components on the magma source. The effect of crustal contamination on the magmas of Group II was higher than Group I. Group I lavas were found to be generated from a more enriched source compared to the lavas of Group II. The magmas from which these lavas were generated were from a lithospheric source and contain garnet residue at various levels. Additionally, the subduction-metasomatized lithosphere is the result of delamination of the thermal boundary layer or slab detachment of the post-collision magmatism. Lithospheric and crustal thicknesses are important parameters that influence the petrogenesis of magma. The lithosphere in the study area measured between 140 and 150 km in thickness while the crustal thickness measured between 40 and 46 km. The lithospheric and crustal thickness contours presented show that the lithosphere and crust in the Nehbandan area are thinnest in the Sistan Suture Zone. Lithospheric thinning beneath the Nehbandan area may be related to recent slab detachment or post-collision extensional delamination. Lithospheric mantle thinning beneath orogenic belts is not an uncommon feature and has also been recorded beneath the Tibetan Plateau and the Atlas Mountains. However, since the alkaline volcanism is restricted to the area formed along the Nehbandan Fault, the melting processes may be related to lateral stretching as well as simple or pure shear stretching. Additionally, consistency between the timing of the Nehbandan Fault and the alkaline magmatism in this area may suggest that localized stretching initiated the melting and produced the alkaline magma.

## References

[1] Alavi- Naini, M., Eftekharnezhad, J. & Aghanabati, A. (1990): Gological map of Zabol, Scale 1/ 250000, Geol. Surv. Iran.

[2] Saccani, E., Delavari, M., Beccaluva, L. & Amini, S. (2010): Petrological and geochemical constraints on the origin of the Nehbandan ophiolitic complex (eastern Iran): Implication for the evolution of the Sistan Ocean. - Lithos 117: 209–228.

[3] Arjmandzadeh, R., Karimpour, M.H., Mazaheri, S.A., Santos, J.F., Medina, J.M., & Homam, S. M. (2011): Two-sided asymmetric subduction; implications for tectonomagmatic and metallogenic evolution of the Lut Block, eastern Iran. - J. Econ. Geol. 1 (3): 1-14.

[4] Hazrati, A., Mehdipour Ghazi, J. & Ketabdari, M.R. (2009): Geochemistry of Eshkaftou granite northwest of Birjand town (Eastern Iran), implication for tectonic environment and origin.- Geol. Soc. Bulgarian Rev. 70: 37-46.

[5] Tirrul, R., Bell, I.R., Griffis, R.J. & Camp, V.E. (1983): The Sistan suture zone of eastern Iran. - Geol. Soc. Am. Bull. 94: 134–150.

[6] Eftekharnejad, J. (1981): Tectonic division of Iran with respect to sedimentary basins. - J. Iranian Petrol. Soc. 82: 19–28.

[7] Berberian, M. (1983): Continental deformation on the Iranian Plateau, G.S.I.No. 52.

[8] Dewey, J. F. (1977): Suture zone complexities:

a review. – Tectonophysics 40: 53—67.

[9] Stocklin, J. S. (1968): Structural history and tectonics of Iran. A review. - Am. Assoc. Petr. Geol. Bull. 52: 1229-1258.

[10] Camp, V.E. & Griffis, R.J. (1982): Character, genesis and tectonic setting of igneous rocks in the Sistan suture zone, eastern Iran. - Lithos 15: 221–239.

[11] Sadeghian, M., Bouchez, J.L., Nédélec, A., Siqueira, R. & Valizadeh, M.V. (2005): The granite pluton of Zahedan (SE Iran): a petrological and magnetic fabric study of a syntectonic sill emplaced in a transtensional setting. – J. Asian Earth Sci. 25: 301–327.

[12] Emami, M. H., Sadeghi, M. M. M. & Omrani, S. J. (1993): Magmatic map of Iran (Tehran). - Geol. Surv. Iran.

[13] Walker, R. T., Gans, P., Allen, M. B., Jackson, J., Khatib, M., Marsh, N. & Zarrinkoub, M. (2009): Late Cenozoic volcanism and rates of active faulting in eastern Iran. - Geophys. J. Int. 177: 783-805.

[14] Jim´enez-Munt, I., Fern`andez, M., Saura, E., Verg´es, J. & Garcia Castellanos, D. (2012): 3-D lithospheric structure and regional/residual Bouguer anomalies in the Arabia–Eurasia collision (Iran). – Geophys. J. Int. 190: 1311- 1324.

[15] Meschede, M. (1986): A method of discriminating between different types of mid-ocean ridge basalts and continental tholeiites with the Nb, Zr, Y diagram. – Chem. Geol. 56: 207–218.

[16] Klein, E. M. & Langmuir, Ch. (1987): Global correlations of ocean ridge basalt chemistry with axial depth and crustal thickness. – J. Geophys. Res. 92: 8089–8115.

[17] Niu, Y., & Batiza, R. (1991): An empirical method for calculating melts compositions produced beneath mid-ocean ridges: application for axis and off-axis (seamounts) melting. – J. Geophys. Res. 96: 21753–21777.

[18] Langmuir, Ch., Klein, E. & Plank, T. (1992): Petrological systematic of mid-ocean ridge basalts: constraints on melt generation beneath ocean ridges. In: Morgan, J., Blackman, D., Sinton, J. (Eds.), Mantle Flow and Melt Generation at Mid-Ocean Ridges. Geophysical Monograph Series. - American. Geophys. Union. 71: 183–277.

[19] Sun, S. S. & McDonough, W. F. (1989): Chemical and isotopic systematics of oceanic basalts: implications for mantle composition and processes. In: A. D. Saunders and M. J. Norry (Eds.), Magmatism in ocean basins. – Geol. Soci. London. Spec. Pub. 313–345.

[20] Boyton, W.V. (1984): Geochemistry of the rare earth elements: meteorite studies. In: HENDERSON, P. (ed), Rare Earth Element Geochemistry, Elsevier. 63–114.

[21] Wilson, M. (1989): Igneous petrogenesis: A Global Tectonic Approach. - Harper Collins Academics, pp. 466.

[22] Muller, D., & Groves, D, I. (1997): Potassic igneous rocks and associated gold-copper mineralization. Springer–Verlag, pp. 242.

[23] Taylor, S.R. & McLennan, S.H. (1985): The continental crust: Its composition and evolution: Blackwell, Oxford, pp. 312.

[24] Sun, C. H. & Stern R. J. (2001): Genesis of Mariana shoshonites; contribution of subduction component. – J. Geophys. Res. Lett. 106: 589-608.

[25] Pearce, J. A., Stern, R. J., Bloomer, S. H. & Fryer, P. (2005): Geochemical mapping of the Mariana arc-basin system: implications for the nature and distribution of subduction components. - Geochem. Geophys. Geosyst. 6, Q07006, Doi: 10.1029/ 2004GC000895.

[26] Norman, M.D. & Garcia, M.O. (1999): Primitive magmas and source characteristics of the Hawaiian plume: petrology and geochemistry of shield picrites. – Earth. Planet. Sci. Lett. 168: 27-44.

[27] Aldanmaz, E., Pearce, J.A., Thirwall, M.F. & Mitchell, J.G. (2000): Petrogenetic evolution of late Cenozoic post-collision volcanism in western Anatolia, Turkey. - J. Volcanol. Geothermal. Res. 102: 67–95.

[28]Alıcı, P., Temel, A. & Gourgaud, A. (2002): Pb-Nd-Sr isotope and trace element geochemistry of Quaternary extension-related alkaline volcanism: a case study of Kula region (western Anatolia, Turkey). - J. Volcanol. Geothermal. Res. 115: 487-510.

[29] McKenzie, D. & O'Nions, R. K. (1991): Partial melt distributions from inversion of rare earth element concentrations. - J. Petrol. 32: 1021–1091.

[30] Pearce, J.A. (1982): Trace element characteristics of lavas from destructive plate boundaries, in Thorpe, R.S., ed., Andesites: New York, Wiley. 525–548.

[31] Shaw, D.M. (1970): Trace element fractionation during anatexis. - Geochim. Cosmochim. Acta 34: 237–243.